THE JOURNAL OF PHYSICAL CHEMISTRY Letters

Letter

Cite This: J. Phys. Chem. Lett. 2018, 9, 2460−2468

pubs.acs.org/JPCL

# Correction Scheme for Comparison of Computed and Experimental Optical Transition Energies in Functionalized Single-Walled Carbon Nanotubes

Brendan J. Gifford,[†,∥,⊥] Andrew E. Sifain,[‡,§,∥] Han Htoon,[⊥] Stephen K. Doorn,[⊥] Svetlana Kilina,[†] and Sergei Tretiak*[,§,∥,⊥]

[†]Department of Chemistry and Biochemistry, North Dakota State University, Fargo, North Dakota 58108, United States

[‡]Department of Physics and Astronomy, University of Southern California, Los Angeles, California 90089, United States

[§]Theoretical Division, [∥]Center for Nonlinear Studies, [⊥]Center for Integrated Nanotechnologies, Materials Physics and Applications Division, Los Alamos National Laboratory, Los Alamos, New Mexico 87545, United States

Supporting Information

**ABSTRACT:** Covalent functionalization of single-walled carbon nanotubes (SWCNTs) introduces red-shifted emission features in the near-infrared spectral range due to exciton localization around the defect site. Such chemical modifications increase their potential use as near-infrared emitters and single-photon sources in telecommunications applications. Density functional theory (DFT) studies using finite-length tube models have been used to calculate their optical transition energies. Predicted energies are typically blue-shifted compared to experiment due to methodology errors including imprecise self-interaction corrections in the density functional and finite-size basis sets. Furthermore, artificial quantum confinement in finite models cannot be corrected by a constant-energy shift since they depend on the degree of exciton localization. Herein, we present a method that corrects the emission energies predicted by time-dependent DFT. Confinement and methodology errors are separately estimated using experimental data for unmodified tubes. Corrected emission energies are in remarkable agreement with experiment, suggesting the value of this straightforward method toward predicting and interpreting the optical features of functionalized SWCNTs.

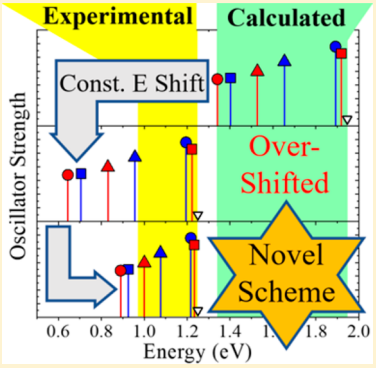


Single-walled carbon nanotubes (SWCNTs) have been a subject of intense investigation since their discovery in 1991[1] due to their chirality-dependent electronic and optical properties,[2,3] which make them useful for a wide range of applications including photovoltaics,[4−7] sensors,[8−13] and light emitting diodes.[14−18] Due to differences in electron confinement along the radial direction of SWCNTs, emission energies vary from approximately 1000 to 1200 nm for nanotubes with diameters between 0.6 and 1.0 nm, respectively. While these diameter-dependent emission properties introduce some degree of tunability in pristine SWCNTs, further modification of their electronic and optical properties can be accomplished through covalent functionalization of the nanotube with small organic molecules.[19]

In particular, SWCNTs functionalized by a low concentration of oxygen[20−23] or aryl species[24−28] form covalent bonds at the sidewall of the SWCNT generating $sp^3$-defects in the $sp^2$-hybridized carbon lattice. This chemical defect, also referred to as a quantum defect[19,21] or a dopant,[23] localizes the excited state electron density by forming a potential well in the immediate vicinity with a depth of 100 to 300 meV.[19,28,29] Thus, the energy splitting and optical selection rules for the lowest-energy excitons are changed[30,31] and dark excitons are brightened.[28,32] Following absorption along the pristine portion of the tube at energy $E_{11,A}$, the exciton becomes trapped at the defect site (*) and undergoes vibrational reorganization and emission[29,33] at energy $E^*_{11,E}$ in the near-infrared range.[20] Due to formation of a deep confinement potential, these defect states are also expected to maintain single photon emission of IR and near-IR wavelengths. In line with this expectation, room temperature single photon emission,[34] as well as tunability of this quantum light emission to 1.55 $\mu$m,[24] has been recently demonstrated. This opens a new path to realize room temperature single photon sources operating at telecommunication wavelengths, since the emission of the defect states can readily be extended to this range via use of larger diameter SWCNTs.[24] The precise energy of emitted photons depends on the position of defects at the nanotube surface, corresponding to different degrees of exciton localization,[25] as well as on the chemical composition of the functional group.[19] Furthermore, functionalization facilitates photon upconversion[35] and stabilizes trions at room temperature,[36] making SWCNTs an attractive material for emergent photonic applications. Realization of this tremendous potential demands

Received: March 1, 2018
Accepted: April 20, 2018
Published: April 20, 2018





DOI: 10.1021/acs.jpclett.8b00653
J. Phys. Chem. Lett. 2018, 9, 2460−2468

a detailed understanding of the electronic structure and chemical nature of the SWCNT defect states.

Density functional theory (DFT) has been widely utilized and shown to be instrumental in predicting and interpreting optical features of covalently functionalized SWCNTs.[21,23,25,30,31,37−39] However, experimental systems are on the order of micrometers in length, which is prohibitively expensive for DFT if periodic boundary conditions are not used.[40−42] Moreover, periodic boundary conditions with small unit cells may introduce spurious interactions between functional groups. Alternative models use finite-length nanotube segments sufficiently long to minimize the effects of artificial quantum confinement introduced by the model. In order to utilize time-dependent DFT (TDDFT) approaches[43] to study the excited state properties, the size of SWCNTs is commonly reduced to nanometer length scales to make them feasible for calculations.[30,37,44,45] To qualitatively replicate the electronic structure of the effective infinite-length SWCNT systems, it is imperative to passivate the dangling bonds at the ends of finite SWCNTs with a scheme involving hydrogen and methylene groups.[44,46] While qualitative trends derived from finite models of SWCNTs may be useful toward analyzing optical features due to chemical modifications, the value of quantitative data is compromised due to several approximations. These include artificial localization of excitons due to tube ends, known as quantum confinement error, and the methodology error introduced by use of an incomplete basis set and self-interaction errors in the density functional. Collectively, these errors tend to blueshift computed optical transitions relative to experimental values.[25] Notably, such blue-shifts are more pronounced for hybrid density functionals, while providing a physically meaningful description of excitonic effects in these materials.[47]

Ideally, energies must be consistently corrected to compare theory to experiment. One method would be to introduce a constant energy shift (or so-called "scissor operation"), as typically applied for conjugated systems such as semiconducting polymers and pristine SWCNTs.[48] While this method is simple, it does not consider the two sources of error independently. Methodology errors are similar across all species (e.g., different tube chiralities), whereas confinement errors depend on the degree of electron localization and may be insignificant for species with excitons strongly localized close to the defect site, as compared to those delocalized across the entire tube. In the latter systems, a constant shift may overestimate energies, since it neglects species-dependent confinement error. As such, a subsequent subtraction of confinement error proportional to the degree to which the exciton is localized would be required. In this case, a proper scheme that corrects transition energies with different degrees of exciton localization must treat confinement and methodology errors independently.

In this paper, we present an approach that corrects energies obtained from TDDFT and allows for direct comparison of the calculated optical spectra with experimental spectra of functionalized SWCNTs. Confinement errors are estimated by considering the length dependence of absorption energies of four different chiralities of SWCNT functionalized by aryls in different configurations, Figure 1. A correlation between extrapolated emission energies at infinite-lengths and redshifts in finite systems is then established. Empirical energy corrections determined solely from experimental emission energies of pristine SWCNTs are used to estimate methodology errors. The proposed method avoids the large computational expense of calculating the excited state properties for very large systems and allows comparing various chosen model chemistries (i.e., DFT functional/basis set) with experimental data. This method is computationally efficient and can be used to correct the computed emission features in functionalized SWCNTs providing quantitative accuracy. Furthermore, this method has potential to be useful in low-dimensional excitonic systems such as quantum dots, 2D materials, and different heterostructures, provided the availability of adequate computational models to track size-dependent trends in electronic excitations. A necessary requisite of this approach is to have reference experimental data for some electronic excitations.

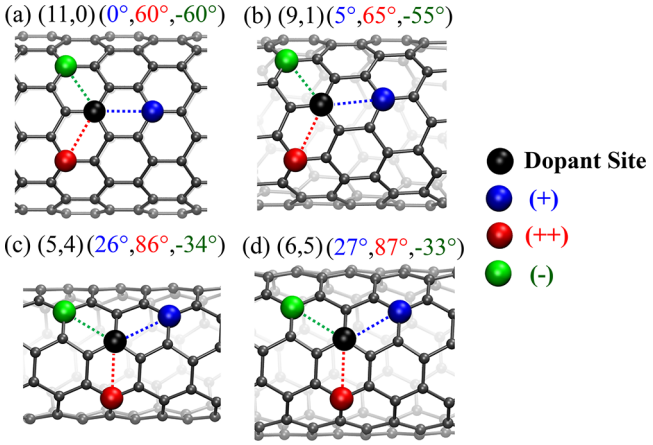


**Figure 1.** Functionalization configuration for (a) (11,0), (b) (9,1), (c) (5,4), and (d) (6,5) SWCNTs. Blue atoms represent the carbon atoms functionalized to place both defects in positions generating a small positive angle with respect to the tube axis. Red and green atoms represent those functionalized to place defects in para positions generating a large positive or negative angle with respect to the axis, respectively. The angles in parentheses represent the approximate angle with respect to the SWCNT axis. See Supporting Information (SI) for ortho configurations.

Four model systems of varying length ranging from 4 to 18 nm were considered for each chirality and configuration (Figure 1). The optical transition energies were calculated for each length to establish scaling relationships between optical transition energies and the extent of the excitons. Adjustment of the resulting relationship to match experimental values of the pristine system enables prediction of emission energies for the functionalized systems (Figure 2). Two density functionals (B3LYP and CAM-B3LYP) were used for this procedure. Due to different components of hybrid exchange, these models provide different values for optical transition energies. While values predicted by B3LYP are more comparable to experimental values, CAM-B3LYP has previously demonstrated superior localization characteristics in functionalized SWCNT systems.[49] The procedure introduced here enables quantitative agreement with experiment while using density functionals that demonstrate qualitatively accurate behavior. For computational efficiency, the minimal STO-3G basis set was utilized for all the calculations. Further details are provided in the Computational Methods section.

Absorption energies at the defect site, $E^{*}_{11,A}$, depend on exciton localization caused by chirality and the configuration of functionalization (Figure 2a−d). The slope of the correlation relates to the dependence of confinement on $E^{*}_{11,A}$. For all chiralities, the greatest slope is observed for $E_{11}$ of the pristine SWCNT, which is expected since these excitons are the most



DOI: 10.1021/acs.jpclett.8b00653
J. Phys. Chem. Lett. 2018, 9, 2460−2468

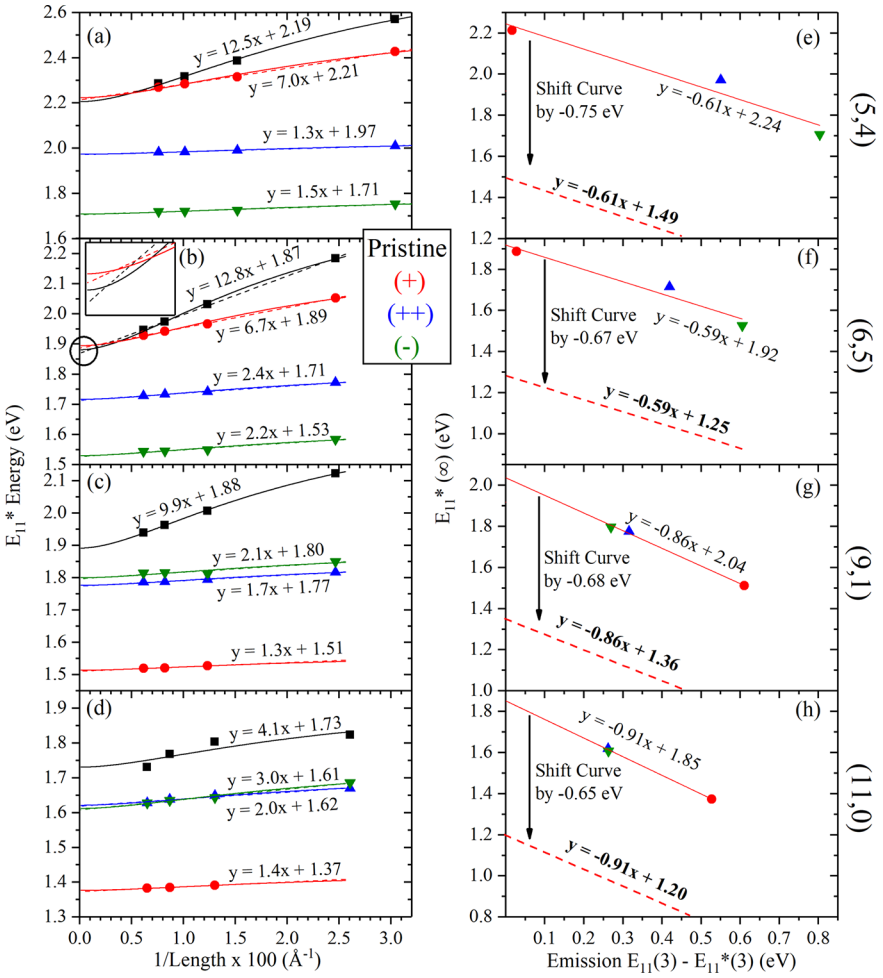


**Figure 2.** (a–d) Correlation between nanotube length and $E^*_{11,A}$ energy for different functional configurations of para-functionalized SWCNTs computed using the CAM-B3LYP density functional. The inset in panel b represents the region centered around the most delocalized species. Dashed and solid lines represent the least-squares linear regression and the fit to Kuhn's formula, respectively. (e–h) Computed redshifts for the emission of the 3-unit cell systems computed with CAM-B3LYP correlated to the intercepts from panels a–d representing $E^*_{11,E}(\infty)$. A constant shift was used such that the *y*-intercept matches experimentally determined values.

delocalized. Covalently bound functional groups localize the exciton around the defect site, where functionalization configurations with the highest exciton localization show the most red-shifted emission (Table 1). The change in $E^*_{11,A}$ with a lengthened system is therefore less significant in the species with the most localized exciton (lowest energy curves in Figure 2a–d), as compared to those with less localization (highest energy curves in Figure 2a–d), reflecting reduced confinement effects. For all chiralities, exciton energies are expected to saturate once the length of the unit cell becomes significantly larger than the size of the exciton. This behavior is observed for all systems beyond three unit cells in length (>15 nm), being the most pronounced for most-localized excitons (Figure 2a–d and Figures S1–S4 in the SI). Due to this saturation, it is assumed that the confinement error estimated for infinitely long SWCNTs is eliminated, providing the basis for deconstructing the methodology and confinement errors independently from each other, as described in the Computational Methods section.

The extrapolated energies at infinite-length are consistent with the previous discussion; localized excitons produce lower absorption energies than delocalized excitons. The only deviation from this trend is observed in near-armchair systems

**Table 1. Notation, Angle of Functionalization with Respect to the SWCNT Axis, and Transition Energies for Different Systems Considered in This Study**[a]

| Chirality | Notation | Functionalization Angle (°) | Para $E^*_{11,E}(3)$ (as calculated, eV) | |
|---|---|---|---|---|
| | | | CAM-B3LYP | B3LYP |
| (5,4) | (+) | 26 | 2.24 | 1.72 |
| | (++) | 86 | 1.70 | 1.37 |
| | (-) | -34 | 1.45 | 1.20 |
| (6,5) | (+) | 27 | 1.92 | 1.45 |
| | (++) | 87 | 1.53 | 1.21 |
| | (-) | -33 | 1.34 | 1.09 |
| (9,1) | (+) | 5 | 1.32 | 1.09 |
| | (++) | 65 | 1.61 | 1.28 |
| | (-) | -55 | 1.66 | 1.31 |
| (11,0) | (+) | 0 | 1.22 | 0.99 |
| | (++) | 60 | 1.48 | 1.16 |
| | (-) | -60 | 1.48 | 1.16 |

[a]The gradient represents the degree of localization in the exciton, where blue and red are least and most localized, respectively.

calculated by CAM-B3LYP, where the energy of pristine $E^*_{11,A}$ drops below $E^*_{11,A}$ of the (+) exciton (inset of Figure 2b). This anomaly is very small (crossover of less than 20 meV) and disappears when calculated with B3LYP (Figures S1c and S2c).



DOI: 10.1021/acs.jpclett.8b00653
J. Phys. Chem. Lett. 2018, 9, 2460–2468

Literature reports have demonstrated dependence of the degree of charge localization on density functionals in both anionic and cationic cycloparaphenylenes, the simplest structural unit of armchair SWCNTs.[33] These systems exhibit maximum charge density near the central portion of the tube when calculated with CAM-B3LYP, and a more homogeneous charge distribution when calculated with B3LYP. In the present study, differences in the correlations between $E^*_{11,A}$ and lengths using both B3LYP and CAM-B3LYP functionals demonstrates that the same observations can be extended to other small-diameter SWCNTs. The slopes in the energy-length correlations for (5,4), (6,5), and (9,1) chiralities are nearly identical for both functionals where excitons are delocalized across the length of the tubes (Figures S1−S4 in the SI). For larger diameter (11,0), the slope is reduced due to a higher degree of localization (Table S2, Figure S5). Dependence of strongly localized $E^*_{11,A}$ on length is generally smaller with CAM-B3LYP than B3LYP for all functionalized SWCNTs, because the B3LYP functional is known for its overestimation of delocalization character of orbitals.[44]

In order to obtain corrections for the computed energies, we approximate emission energies by absorption energies extrapolated at infinite-length. Such an approximation is valid due to sufficiently small Stokes shifts observed in nanotubes.[45] Additionally, our previous studies demonstrate that calculations of the lowest optically active states in absorption spectra provide a qualitatively correct description of emission transitions in both pristine and functionalized SWCNTs.[45] Next, the emission energies at the infinite-length limit are linearly correlated to the $E_{11,E}(3)-E^*_{11,E}(3)$ redshifts in SWCNTs of three unit cells in length, as presented in Figure 2e−h. The $E_{11,E}(\infty)$ transitions for pristine SWCNTs are defined for $E_{11,E}(3) - E^*_{11,E}(3) \approx 0$ and are aligned with those determined from experiment.[50] The Computational Methods section presents further discussion of this procedure.

Notably, $E_{11,E}(\infty)$ varies for different diameter tubes consistent with exciton confinement in the dimensions perpendicular to the SWCNT axis and exhibits the same degree of diameter dependence as experimental values[50] (Figure 3a). The pristine (11,0) systems exhibit the least amount of confinement along circumference due to their larger diameter and therefore exhibit the smallest emission energies. Conversely, (5,4) systems exhibit more circumferential confinement and larger emission energies. These well-established trends are similar for both extrapolated $E_{11,E}(\infty)$ and $E_{11,E}(3)$ taken directly from three unit-cell calculations, while slightly higher values of $E_{11,E}(3)$ originated from the axial confinement effect. Differences between $E_{11,E}(\infty)$ and $E_{11,E}(3)$ are in the range from 0.04 to 0.14 eV, nearly independent of density functional (Figure 3b). Furthermore, the magnitudes of these differences are diameter dependent. However, the step-like trend between near-armchair or near-zigzag tubes is less pronounced in calculations with three unit cells, but is evident in extrapolated energies, especially when calculated using B3LYP functional (Figure 3a).

The extrapolated energies plotted against the calculated energies of emission features generates the correlation that is subsequently used for correcting the calculated emission values. These are presented in the right panels of Figure 2. The magnitude of the slopes reflect the degree to which confinement versus methodology errors affect computed results. When the slope is significantly smaller than 1 (as in the near-armchair systems), more error originates from

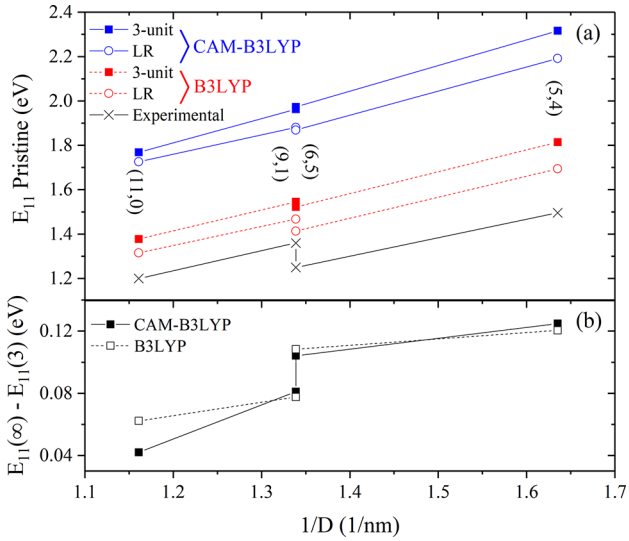


**Figure 3.** (a) Calculated $E_{11}$ energies for pristine SWCNTs of different diameter and chirality, including (11,0), (9,1), (6,5), and (5,4). Solid square points represent the energies as calculated using three unit cell computational cells, while the open circles represent the energies extrapolated from the infinite length linear regressions (LR) of length dependence of $E_{11}$. Blue and red points represent those calculated using CAM-B3LYP versus B3LYP, respectively. Black (×) points represent the experimental values to which all trends were shifted for the purpose of correcting the computed values. (b) Difference between the $E_{11}$ as calculated from three unit cell long systems versus the linear regression, using either CAM-B3LYP (open data points) or B3LYP (closed data points).

confinement, which affects the transition energies for functionalization configurations with localized excitons to a lower degree than those with delocalized excitons. A slope close to 1 indicates confinement errors are less significant compared to methodology errors. Thus, a constant energy shift contributing mainly from the methodology error dominates in (9,1) and (11,0) systems. As such, we define the methodology error as a difference between the experimental energy of the main $E_{11}$ band of the pristine SWCNT and the extrapolated $E_{11}$ energy of an infinitely long nanotube model for the most localized systems (calculated with eq 3 and illustrated in Figure S6). It results in the constant red-shift of $E^*_{11,E}$ for each functionalized SWCNT, with the value depending on the tube chirality and the DFT functional, as shown in Figure 4.

Overestimation of HOMO−LUMO gaps and emission energies using CAM-B3LYP has been well documented.[48] The same is observed in Figure 4 for all functionalization configurations: methodology errors are roughly 0.4 to 0.6 eV with CAM-B3LYP and 0.05 to 0.15 eV with B3LYP, depending on tube chirality. Confinement errors, calculated by eq 4 (see Computational Methods) and defined as the difference between the total shift introduced by our method and the methodology error for each species, are also greater with CAM-B3LYP. Magnitudes of about half the methodology error in near-armchair systems with delocalized excitons are observed, resulting in significant blue shifts relative to experiment. However, any effect that localizes the exciton generally decreases confinement errors. For example, functionalization configurations that generate localized excitons exhibit less significant confinement errors. Furthermore, use of B3LYP results in confinement errors exceeding methodology errors


DOI: 10.1021/acs.jpclett.8b00653
J. Phys. Chem. Lett. 2018, 9, 2460−2468

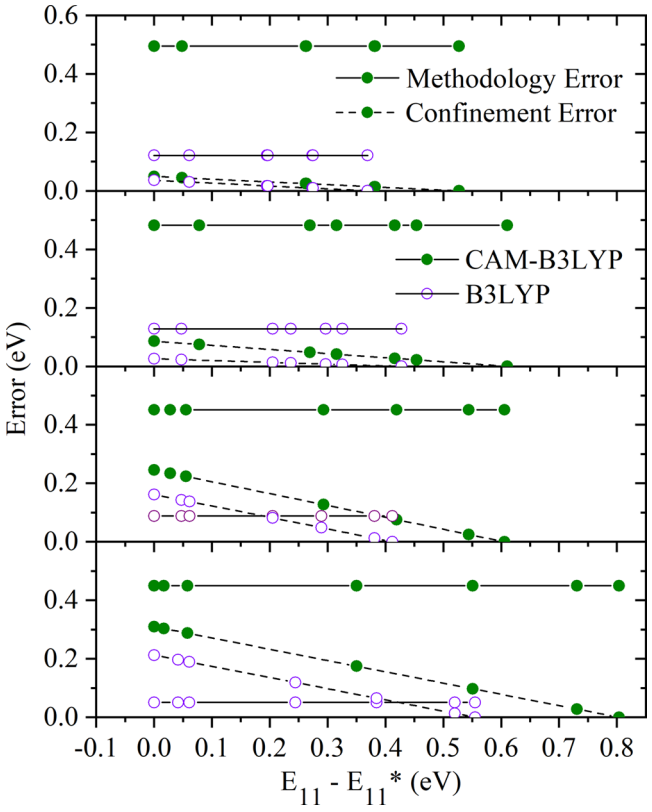


**Figure 4.** Methodology and confinement errors as a function of the $E_{11}$* exciton shift from the main $E_{11}$ exciton for aryl-functionalized (a) (11,0), (b) (9,1), (c) (6,5), and (d) (5,4) SWCNTs. Green lines represent methodology errors, while magenta lines represent confinement errors. Green lines represent methodology errors, while magenta lines represent confinement errors. These errors were calculated using eqs 3 and 4 for methodology and confinement errors, respectively. Solid lines represent the errors with CAM-B3LYP, while dashed lines are for B3LYP.

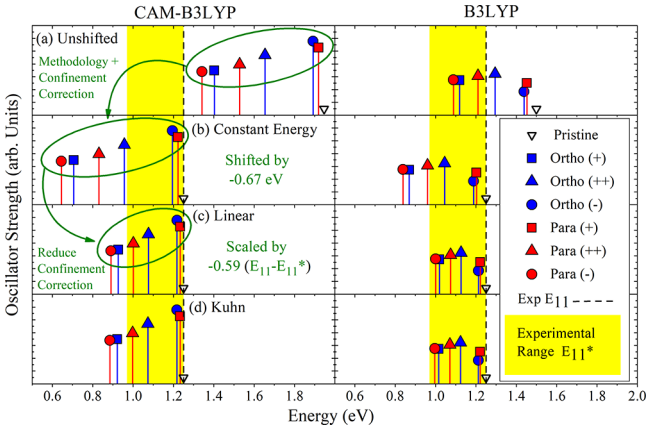


**Figure 5.** Computed energies of $E^*_{11,E}$ for the six different functional configurations of aryl-functionalized (6,5) SWCNTs (a) as calculated using the specified methodology, (b) shifted by a constant energy value, (c) corrected for confinement errors using linear regression to determine the effect of exciton localization on $E^*_{11,E}$, and (d) by using a fit to Kuhn's formula to determine the effect of exciton localization on $E^*_{11,E}$. Square, triangular, and circular markers represent functionalization along the (+), (++), and (−) configurations, respectively. Blue markers denote values for ortho functionalization, while red markers denote para. The left and right columns present the results as calculated using CAM-B3LYP and B3LYP, respectively. The area highlighted in yellow is the range of energies where emission features were observed experimentally, and the dashed vertical lines represent the experimental $E_{11,E}$ of pristine SWCNTs.

due to overlocalization of orbitals using this method. By contrast, similar systems calculated with CAM-B3LYP results in methodology errors always exceeding confinement errors, independent of the functionalization configuration. This can be rationalized by overestimated exciton energies and more localized character of orbitals, compared to those calculated by the B3LYP functional. Confinement errors are slightly reduced for near-zigzag systems when estimated by fitting to Kuhn's eq (eq 1, Computational Methods). This has been used to describe the length dependence of the optical properties in conjugated polymers. Because of the pseudo one-dimensional structure of these systems, we would expect Kuhn's formula to better approximate optical properties dependent on length in SWCNTs. However, the relative contribution of each type of error is independent of the fitting method (Figure S7 and S8). Further discussion of the differences between results from trends generated using a linear regression versus Kuhn fitting can be found in the Supporting Information.

Previous studies attribute the diversity of emission energies of functionalized SWCNTs to the presence of distinct chemical configurations.[25,45] Due to the combined effect of confinement and methodology errors, practically all of the uncorrected emission energies calculated with CAM-B3LYP are higher than experimental energies $E_{11,E}$. These blueshifts may exceed 0.50 eV for all chiralities (Figures 5a and S9a-S11a), indicative of the significant methodology errors with this density functional. Following a constant energy shift, some emission energies fall within the experimentally observed range (Figure 5b). Solely shifting by a constant energy overcorrects defect-associated emission features due to the role of confinement errors in these systems relative to species with localized excitons. Shifting energies according to the method developed here, which includes both confinement and methodology errors, significantly improves agreement with experiment regardless if extrapolated energies were determined from linear or Kuhn scaling (Figures 5c,d). Smaller methodology errors associated with B3LYP puts calculated energies in closer proximity to experiment, where $E_{11,E}(\infty)$ is blue-shifted from experiment only by about 0.25 eV, compared to 0.65 eV shift for CAM-B3LYP calculations (Figure 5b). This is because B3LYP provides lower degrees of charge localization resulting in smaller methodology errors relative to those determined with CAM-B3LYP. However, fully corrected energies, including both methodology and confinement corrections, are within the experimental range. As such, this correlation approach only weakly depends on the nature of the underlying DFT model.

In conclusion, a correction scheme accounting for errors due to both electronic structure methodology and quantum confinement in finite-size covalently functionalized SWCNTs was developed. This approach enables calculation of accurate emission energies as compared to experimental data using only the experimental value of the excitonic transition energy $E_{11}$ in pristine (nonfunctionalized) SWCNTs. The validity of this correction scheme has been demonstrated using TDDFT methodology for excited state calculations of four nanotube chiralities ((5,4), (6,5), (9,1) and (11,0)), each chemically functionalized with aryl groups at six experimentally feasible but topologically distinct configurations.[25,45] These corrections utilize numerically inexpensive vertical transition energies



DOI: 10.1021/acs.jpclett.8b00653
J. Phys. Chem. Lett. 2018, 9, 2460−2468

calculated for ground-state optimized geometries of SWCNTs of several different lengths. Length dependence of absorption energies is further fit to linear and Kuhn's formula. Notably, a simpler linear fit gives nearly indistinguishable results. As expected, confinement corrections are affected by the degree of exciton localization around the defect site, which in turn depends on the binding configuration and/or density functional used. Transition energies for systems with localized excitons quickly saturate with the tube length. Therefore, energy deviations in species with highly localized excitons around the defect sites are solely due to methodology errors. We find that methodology errors by far exceed confinement errors in calculations using the CAM-B3LYP functional. By contrast, these errors are approximately equal in magnitude when using the B3LYP model. Due to defect-dependent discrepancies in the degree of methodology versus confinement error, a constant energy shift is insufficient for correcting calculated energies to match experiment. By contrast, our proposed method shows improved correction, independent of exciton localization. Regardless of configuration, the degree to which methodology and confinement errors affect the results is dependent on exciton localization within the species. Therefore, the correction method presented here is valid for any chirality and defect conformation. In fact, corrected emission energies of functionalized (6,5) SWCNTs are in excellent agreement with recently published experimental data.[25] Moreover, the end result is nearly agnostic to the density functional used, allowing for consistent comparison with experiment for different computational methodologies. We believe that this approach improves the predictive power of quantum-chemical calculations of excited states in chemically modified SWCNTs toward realizing a theory-guided materials design paradigm. This method has further potential to be useful in a variety of other low-dimensional excitonic systems such as quantum dots, 2D materials, and different heterostructures.

## COMPUTATIONAL METHODS

Four SWCNTs of (5,4), (6,5), (9,1) and (11,0) chirality with one to four unit-cells in length were constructed using the Visual Molecular Dynamics (VMD) software.[51] The dangling bonds at the end of the computational cell were passivated with a mixture of hydrogen and methylene groups using schemes that have been previously shown to eliminate midgap trap states and properly approximate the scaling-relationships for infinite length systems (Table S1).[44] The pristine SWCNTs were functionalized with aryl and hydrogen groups in ortho and para positions, consistent with the synthetically relevant species established by previous studies.[25,45] These groups are arranged across the six-membered ring from each other and along three distinct orientations with respect to the SWCNT axis (Figure 1). For example, for (6,5) SWCNTs, these positions are denoted by $L_{30}$, $L_{90}$, and $L_{-30}$, where the subscript is the approximate angle between the vector connecting the two functionalized carbon atoms and the SWCNT axis, as previously defined in the literature.[25,45] For purposes of comparing functionalized configurations across different chiralities, the smallest and largest positive angle with respect to the axis of the SWCNT are labeled (+) and (++) respectively, while the negative angle with respect to the SWCNT axis is labeled (−). Para configurations cover the entire energy range of emission features and capture the same localization-emission redshift behavior as ortho. Therefore, only para configurations were considered for establishing scaling factors in this report.

Geometries of all structures were optimized with DFT using the CAM-B3LYP[52] density functional and a STO-3G basis set.[53] These methodologies have previously been shown to be in reasonable agreement with experiment.[37,48] The predicted energies of optical transitions have been previously shown to be qualitatively independent of basis set size, and quantitative agreement can be achieved by introducing a constant energy shift.[45] As such, the methodology correction developed here corrects for errors originating from basis set size as well. Vertical transitions were calculated from the ground-state optimized geometries of all functionalized configurations. This level of theory has been effective in predicting emission energies of functionalized SWCNTs.[25] It is worth noting that while previous calculations using B3LYP (a hybrid functional with a relatively small fraction of orbital exchange 20%) predict emission energies more consistent with experiment,[37] CAM-B3LYP (a range-corrected functional with a large fraction of orbital exchange, 20%−65%) was shown to better describe excitonic effects.[33,47] Since this study seeks to predict properties explicitly considering various localization phenomena, both CAM-B3LYP and B3LYP[54] density functionals were used to predict optical properties. Given the large computational expense, DFT is only possible for SWCNTs up to approximately 16 nm in length. Excited-state optimized geometries, which are required to model emission features, are significantly more expensive and thus can only be used on even shorter systems. All functionalized configurations and pristine SWCNTs, except for (11,0), were optimized in the excited state using only three unit cells (~10 nm). Due to much smaller size of the unit cell of (11,0) SWCNTs, we used 27 unit cells to reach ~10 nm length. This length is expected to be enough to avoid spurious interaction of excitons with tube edges, since the experimental exciton size is about 2 nm in pristine SWCNTs.[48] The emission energies, $E^*_{11,E}(3)$, were determined by calculating vertical transition energies from the optimized excited-state geometries.[55,56] All DFT and TDDFT calculations were performed using Gaussian 09[57] software.

Confinement errors in calculated absorption energies $E^*_{11,A}$ were quantified by considering several SWCNTs of varying length from ~4 nm to ~16 nm. We are quantifying the length dependence on absorption as opposed to emission, since computational costs required to optimize excited-state geometries are too large for SWCNTs over three unit cells, while the confinement errors are expected to affect both quantities in a similar fashion.[42] Using calculated transition energies at finite lengths, we extrapolate absorption energies of infinite-length systems. This extrapolation was performed using both a linear regression and Kuhn's formula.[58,59] The latter describes the length dependence of optical transitions in one-dimensional conjugated polymers and is given by

$$E^*_{11,A}(N) = A\sqrt{1 + B\cos\left(\frac{\pi}{N+1}\right)} \quad (1)$$

where $E^*_{11,A}(N)$ is absorption at the defect site, $N$ is length in units cells, $A$ and $B$ are fitting parameters, and $E^*_{11,A}(\infty) = A\sqrt{1+B}$ is the extrapolated energy at infinite tube length. Taking into account that Stokes shifts, $E^*_{11,A} - E^*_{11,E}$, are relatively small in realistic rigid nanotube systems,[45] emission energies at infinite lengths are approximated as $E^*_{11,E}(\infty) = E^*_{11,A}(\infty)$ and determined in the following way:



DOI: 10.1021/acs.jpclett.8b00653
J. Phys. Chem. Lett. 2018, 9, 2460−2468

$$E^*_{11,E}(\infty) = E^{exp}_{11,E} - \alpha(E_{11,E}(3) - E^*_{11,E}(3)) \quad (2)$$

where $\alpha$ is a slope estimated from the dependence of $E^*_{11,E}$ on the tube length (Figures 2 and S1 to S4), $E_{11,E}(3)$ and $E_{11,E}{}^*(3)$ are the calculated emission energies of tube models of ~10 nm in length corresponding to three unit cells, and $E^{exp}_{11,E}$ is the experimental value of emission energies in pristine SWCNTs taken from ref 50. This approximation is valid since the vibrational reorganization energies at the defect site are sufficiently small as compared to overall redshifts, $\Delta E = E_{11,E}(\infty) - E^*_{11,E}(\infty)$, where $E_{11,E}$ $(\infty)$ is the estimated emission energy of the infinitely long pristine SWCNT.[29,45] This allows us to approximately account for these effects in the constant energy shifts.

Since the confinement insignificantly impacts the energy of localized excitons in tubes of length larger than 10 nm in length (Figure 2 and S1 to S4), we assume that only methodology error contributes in these systems while confinement error can be neglected. As such, we estimate methodology errors using the emission energy of the most localized exciton, $E^{*loc}_{11,E}$ (3), in each functionalized SWCNT as following:

$$\Delta E_{method} = E^{*loc}_{11,E}(3) - E^*_{11,E}(\infty) \quad (3)$$

Given $\Delta E_{method}$, we estimate confinement errors across various defect positions and different tube chiralities as

$$\Delta E_{confinement} = E^*_{11,E}(3) - E^*_{11,E}(\infty) - E_{method} \quad (4)$$

This approach allows for estimating the collective contribution of methodology and confinement errors in SWCNT optical transitions with different degrees of exciton localization.

## ■ ASSOCIATED CONTENT

### Supporting Information

The Supporting Information is available free of charge on the ACS Publications website at DOI: 10.1021/acs.jpclett.8b00653.

Structural characteristics of varied-length functionalized SWCNT systems; length dependence of excitation energies, and regressions of excitation energies for infinite-length aryl-functionalized SWCNTs of (5,4) chirality; length dependence of excitation energies, and regressions of excitation energies for infinite-length aryl-functionalized SWCNTs of (6,5) chirality; length dependence of excitation energies, and regressions of excitation energies for infinite-length aryl-functionalized SWCNTs of (9,1) chirality; length dependence of excitation energies, and regressions of excitation energies for infinite-length systems for aryl-functionalized SWCNTs of (11,0) chirality; parameters for fitting functions of length-dependent emission properties for aryl-functionalized SWCNTs of different chiralities; plot of the slopes and intercepts for a linear regression of the fitting parameters; visual representation of the quantities assigned to methodology and confinement errors for the systems in this study; comparison of the confinement and methodology errors introduced for calculations with both the CAM-B3LYP and B3LYP density functionals; comparison of the energies of infinite-length transition energies extrapolated both with a linear regression and Kuhn's formula; predicted energies of emission features for (5,4) SWCNTs functionalized in various configurations using different fitting functions; predicted energies of emission features for (9,1) SWCNTs functionalized in various configurations using different fitting functions; predicted energies of emission features for (11,0) SWCNTs functionalized in various configurations using different fitting functions (PDF)

## ■ AUTHOR INFORMATION


### Corresponding Author

*E-mail: serg@lanl.gov.

### ORCID

Brendan J. Gifford: 0000-0002-4116-711X
Andrew E. Sifain: 0000-0002-2964-1923
Han Htoon: 0000-0003-3696-2896
Stephen K. Doorn: 0000-0002-9535-2062
Svetlana Kilina: 0000-0003-1350-2790
Sergei Tretiak: 0000-0001-5547-3647


### Notes

The authors declare no competing financial interest.

## ■ ACKNOWLEDGMENTS

This work was conducted, in part, at the Center for Nonlinear Studies and the Center for Integrated Nanotechnologies, U.S. Department of Energy, Office of Basic Energy Sciences user facilities and supported in part by Los Alamos National Laboratory (LANL) Directed Research and Development Funds. S.K. acknowledges NSF Grant CHE-1413614 for financial support of studies of functionalized carbon nanotubes and the Alfred P. Sloan Research Fellowship BR2014-073 for partial support of studies of surface effects at interfaces of nanostructures. For computational resources and administrative support, S.K. and B.G. thank the Center for Computationally Assisted Science and Technology (CCAST) at North Dakota State University and the National Energy Research Scientific Computing Center (NERSC) allocation awards 86678, supported by the Office of Science of the DOE under Contract No. DE-AC02-05CH11231. We also acknowledge the LANL Institutional Computing (IC) Program for providing computational resources.

## ■ REFERENCES


(1) Iijima, S. Helical Microtubules of Graphitic Carbon. *Nature* **1991**, *354* (6348), 56−58.

(2) Saito, R.; Dresselhaus, G.; Dresselhaus, M. S. *Physical Properties of Carbon Nanotubes*; Imperial College Press: London, U.K., 1998.

(3) Dass, D.; Prasher, R.; Vaid, R. Analytical Study Of Unit Cell And Molecular Structures Of Single Walled Carbon Nanotubes. *Int. J. Comput. Eng. Res.* **2012**, *2*, 1447−1457.

(4) Cataldo, S.; Salice, P.; Menna, E.; Pignataro, B. Carbon Nanotubes and Organic Solar Cells. *Energy Environ. Sci.* **2012**, *5*, 5919−5940.

(5) Brown, P.; Takechi, K.; Kamat, P. V. Single-Walled Carbon Nanotube Scaffolds for Dye-Sensitized Solar Cells. *J. Phys. Chem. C* **2008**, *112*, 4776−4782.

(6) Arnold, M. S.; Blackburn, J. L.; Crochet, J. J.; Doorn, S. K.; Duque, J. G.; Mohite, A.; Telg, H. Recent Developments in the Photophysics of Single-Walled Carbon Nanotubes for Their Use as Active and Passive Material Elements in Thin Film Photovoltaics. *Phys. Chem. Chem. Phys.* **2013**, *15*, 14896.

(7) Blackburn, J. L. Semiconducting Single-Walled Carbon Nanotubes in Solar Energy Harvesting. *ACS Energy Lett.* **2017**, *2*, 1598−1613.

(8) Li, J.; Lu, Y.; Ye, Q.; Cinke, M.; Han, J.; Meyyappan, M. Carbon Nanotube Sensors for Gas and Organic Vapor Detection. *Nano Lett.* **2003**, *3*, 929−933.




DOI: 10.1021/acs.jpclett.8b00653
J. Phys. Chem. Lett. 2018, 9, 2460−2468

(9) Zhang, W.-D.; Zhang, W.-H. Carbon Nanotubes as Active Components for Gas Sensors. *J. Sens.* **2009**, *2009*, 1−16.
(10) Zhang, T.; Nix, M. B.; Yoo, B.-Y.; Deshusses, M. A.; Myung, N. V. Electrochemically Functionalized Single-Walled Carbon Nanotube Gas Sensor. *Electroanalysis* **2006**, *18*, 1153−1158.
(11) Wang, Y.; Yeow, J. T. W. A Review of Carbon Nanotubes-Based Gas Sensors. *J. Sens.* **2009**, *2009*, 1−24.
(12) Chen, T.; Wei, L.; Zhou, Z.; Shi, D.; Wang, J.; Zhao, J.; Yu, Y.; Wang, Y.; Zhang, Y. Highly Enhanced Gas Sensing in Single-Walled Carbon Nanotube-Based Thin-Film Transistor Sensors by Ultraviolet Light Irradiation. *Nanoscale Res. Lett.* **2012**, *7*, 644.
(13) Dhall, S.; Jaggi, N.; Nathawat, R. Functionalized Multiwalled Carbon Nanotubes Based Hydrogen Gas Sensor. *Sens. Actuators, A* **2013**, *201*, 321−327.
(14) Zhang, D.; Ryu, K.; Liu, X.; Polikarpov, E.; Ly, J.; Tompson, M. E.; Zhou, C. Transparent, Conductive, and Flexible Carbon Nanotube Films and Their Application in Organic Light-Emitting Diodes. *Nano Lett.* **2006**, *6*, 1880−1886.
(15) Bansal, M.; Srivastava, R.; Lal, C.; Kamalasanan, M. N.; Tanwar, L. S. Carbon Nanotube-Based Organic Light Emitting Diodes. *Nanoscale* **2009**, *1*, 317−330.
(16) Mueller, T.; Kinoshita, M.; Steiner, M.; Perebeinos, V.; Bol, A. A.; Farmer, D. B.; Avouris, P. Efficient Narrow-Band Light Emission from a Single Carbon Nanotube P−n Diode. *Nat. Nanotechnol.* **2010**, *5*, 27−31.
(17) Wang, S.; Zeng, Q.; Yang, L.; Zhang, Z.; Wang, Z.; Pei, T.; Ding, L.; Liang, X.; Gao, M.; Li, Y.; et al. High-Performance Carbon Nanotube Light-Emitting Diodes with Asymmetric Contacts. *Nano Lett.* **2011**, *11*, 23−29.
(18) Bahena-Garrido, S.; Shimoi, N.; Abe, D.; Hojo, T.; Tanaka, Y.; Tohji, K. Plannar Light Source Using a Phosphor Screen with Single-Walled Carbon Nanotubes as Field Emitters. *Rev. Sci. Instrum.* **2014**, *85*, 104704.
(19) Kwon, H.; Furmanchuk, A.; Kim, M.; Meany, B.; Guo, Y.; Schatz, G. C.; Wang, Y. Molecularly Tunable Fluorescent Quantum Defects. *J. Am. Chem. Soc.* **2016**, *138*, 6878−6885.
(20) Ghosh, S.; Bachilo, S. M.; Simonette, R. A.; Beckingham, K. M.; Weisman, R. B. Oxygen Doping Modifies Near-Infrared Band Gaps in Fluorescent Single-Walled Carbon Nanotubes. *Science* **2010**, *330*, 1656−1659.
(21) Ma, X.; Adamska, L.; Yamaguchi, H.; Yalcin, S. E.; Tretiak, S.; Doorn, S. K.; Htoon, H. Electronic Structure and Chemical Nature of Oxygen Dopant States in Carbon Nanotubes. *ACS Nano* **2014**, *8*, 10782−10789.
(22) Miyauchi, Y.; Iwamura, M.; Mouri, S.; Kawazoe, T.; Ohtsu, M.; Matsuda, K. Brightening of Excitons in Carbon Nanotubes on Dimensionality Modification. *Nat. Photonics* **2013**, *7*, 715−719.
(23) Hartmann, N. F.; Yalcin, S. E.; Adamska, L.; Hároz, E. H.; Ma, X.; Tretiak, S.; Htoon, H.; Doorn, S. K. Photoluminescence Imaging of Solitary Dopant Sites in Covalently Doped Single-Wall Carbon Nanotubes. *Nanoscale* **2015**, *7*, 20521−20530.
(24) He, X.; Hartmann, N. F.; Ma, X.; Kim, Y.; Ihly, R.; Blackburn, J. L.; Gao, W.; Kono, J.; Yomogida, Y.; Hirano, A.; et al. Tunable Room-Temperature Single-Photon Emission at Telecom Wavelengths from $Sp^3$ Defects in Carbon Nanotubes. *Nat. Photonics* **2017**, *11*, 577−582.
(25) He, X.; Gifford, B. J.; Hartmann, N. F.; Ihly, R.; Ma, X.; Kilina, S. V.; Luo, Y.; Shayan, K.; Strauf, S.; Blackburn, J. L.; et al. Low-Temperature Single Carbon Nanotube Spectroscopy of $Sp^3$ Quantum Defects. *ACS Nano* **2017**, *11*, 10785−10796.
(26) Powell, L. R.; Piao, Y.; Wang, Y. Optical Excitation of Carbon Nanotubes Drives Localized Diazonium Reactions. *J. Phys. Chem. Lett.* **2016**, *7*, 3690−3694.
(27) Hartmann, N. F.; Velizhanin, K. A.; Haroz, E. H.; Kim, M.; Ma, X.; Wang, Y.; Htoon, H.; Doorn, S. K. Photoluminescence Dynamics of Aryl Sp3 Defect States in Single-Walled Carbon Nanotubes. *ACS Nano* **2016**, *10*, 8355−8365.
(28) Piao, Y.; Meany, B.; Powell, L. R.; Valley, N.; Kwon, H.; Schatz, G. C.; Wang, Y. Brightening of Carbon Nanotube Photoluminescence through the Incorporation of Sp3 Defects. *Nat. Chem.* **2013**, *5*, 840−845.
(29) Kim, M.; Adamska, L.; Hartmann, N. F.; Kwon, H.; Liu, J.; Velizhanin, K. A.; Piao, Y.; Powell, L. R.; Meany, B.; Doorn, S. K.; et al. Fluorescent Carbon Nanotube Defects Manifest Substantial Vibrational Reorganization. *J. Phys. Chem. C* **2016**, *120*, 11268−11276.
(30) Kilina, S.; Ramirez, J.; Tretiak, S. Brightening of the Lowest Exciton in Carbon Nanotubes via Chemical Functionalization. *Nano Lett.* **2012**, *12*, 2306−2312.
(31) Ramirez, J.; Mayo, M. L.; Kilina, S.; Tretiak, S. Electronic Structure and Optical Spectra of Semiconducting Carbon Nanotubes Functionalized by Diazonium Salts. *Chem. Phys.* **2013**, *413*, 89−101.
(32) Wang, Q. H.; Strano, M. S. Carbon Nanotubes: A Bright Future for Defects. *Nat. Chem.* **2013**, *5*, 812−813.
(33) Adamska, L.; Nayyar, I.; Chen, H.; Swan, A. K.; Oldani, N.; Fernandez-Alberti, S.; Golder, M. R.; Jasti, R.; Doorn, S. K.; Tretiak, S. Self-Trapping of Excitons, Violation of Condon Approximation, and Efficient Fluorescence in Conjugated Cycloparaphenylenes. *Nano Lett.* **2014**, *14*, 6539−6546.
(34) Ma, X.; Hartmann, N. F.; Baldwin, J. K. S.; Doorn, S. K.; Htoon, H. Room-Temperature Single-Photon Generation from Solitary Dopants of Carbon Nanotubes. *Nat. Nanotechnol.* **2015**, *10*, 671−675.
(35) Akizuki, N.; Aota, S.; Mouri, S.; Matsuda, K.; Miyauchi, Y. Efficient Near-Infrared up-Conversion Photoluminescence in Carbon Nanotubes. *Nat. Commun.* **2015**, *6*, 8920.
(36) Brozena, A. H.; Leeds, J. D.; Zhang, Y.; Fourkas, J. T.; Wang, Y. Controlled Defects in Semiconducting Carbon Nanotubes Promote Efficient Generation and Luminescence of Trions. *ACS Nano* **2014**, *8*, 4239−4247.
(37) Kilina, S.; Badaeva, E.; Piryatinski, A.; Tretiak, S.; Saxena, A.; Bishop, A. R. Bright and Dark Excitons in Semiconductor Carbon Nanotubes: Insights from Electronic Structure Calculations. *Phys. Chem. Chem. Phys.* **2009**, *11*, 4113−4123.
(38) Zhang, Y.; Valley, N.; Brozena, A. H.; Piao, Y.; Song, X.; Schatz, G. C.; Wang, Y. Propagative Sidewall Alkylcarboxylation That Induces Red-Shifted Near-IR Photoluminescence in Single-Walled Carbon Nanotubes. *J. Phys. Chem. Lett.* **2013**, *4*, 826−830.
(39) Cho, E.; Shin, S.; Yoon, Y.-G. First-Principles Studies on Carbon Nanotubes Functionalized with Azomethine Ylides. *J. Phys. Chem. C* **2008**, *112*, 11667−11672.
(40) Kryjevski, A.; Gifford, B.; Kilina, S.; Kilin, D. Theoretical Predictions on Efficiency of Bi-Exciton Formation and Dissociation in Chiral Carbon Nanotubes. *J. Chem. Phys.* **2016**, *145*, 154112.
(41) Kryjevski, A.; Mihaylov, D.; Gifford, B.; Kilin, D. Singlet Fission in Chiral Carbon Nanotubes: Density Functional Theory Based Computation. *J. Chem. Phys.* **2017**, *147*, 034106.
(42) Erck, A.; Sapp, W.; Kilina, S.; Kilin, D. Photoinduced Charge Transfer at Interfaces of Carbon Nanotube and Lead Selenide Nanowire. *J. Phys. Chem. C* **2016**, *120*, 23197−23206.
(43) Van Caillie, C.; Amos, R. D. Geometric Derivatives of Density Functional Theory Excitation Energies Using Gradient-Corrected Functionals. *Chem. Phys. Lett.* **2000**, *317*, 159−164.
(44) Kilina, S.; Tretiak, S. Excitonic and Vibrational Properties of Single-Walled Semiconducting Carbon Nanotubes. *Adv. Funct. Mater.* **2007**, *17*, 3405−3420.
(45) Gifford, B. J.; Kilina, S. V.; Htoon, H.; Doorn, S. K.; Tretiak, S. Exciton Localization and Optical Emission in Aryl Functionalized Carbon Nanotubes. *J. Phys. Chem. C* **2018**, *122*, 1828.
(46) Sharma, A.; Gifford, B. J.; Kilina, S. Tip Functionalization of Finite Single-Walled Carbon Nanotubes and Its Impact on the Ground and Excited State Electronic Structure. *J. Phys. Chem. C* **2017**, *121*, 8601−8612.
(47) Igumenshchev, K. I.; Tretiak, S.; Chernyak, V. Y. Excitonic Effects in a Time-Dependent Density Functional Theory. *J. Chem. Phys.* **2007**, *127*, 114902.
(48) Kilina, S.; Kilin, D.; Tretiak, S.; Light-Driven. and Phonon-Assisted Dynamics in Organic and Semiconductor Nanostructures. *Chem. Rev.* **2015**, *115*, 5929−5978.


DOI: 10.1021/acs.jpclett.8b00653
*J. Phys. Chem. Lett.* 2018, 9, 2460−2468

(49) Adamska, L.; Nazin, G. V.; Doorn, S. K.; Tretiak, S. Self-Trapping of Charge Carriers in Semiconducting Carbon Nanotubes: Structural Analysis. *J. Phys. Chem. Lett.* **2015**, *6*, 3873−3879.
(50) Weisman, R. B.; Bachilo, S. M. Dependence of Optical Transition Energies on Structure for Single-Walled Carbon Nanotubes in Aqueous Suspension: An Empirical Kataura Plot. *Nano Lett.* **2003**, *3*, 1235−1238.
(51) Humphrey, W.; Dalke, A.; Schulten, K. VMD − Visual Molecular Dynamics. *J. Mol. Graphics* **1996**, *14*, 33−38.
(52) Yanai, T.; Tew, D. P.; Handy, N. C. A New Hybrid Exchange−correlation Functional Using the Coulomb-Attenuating Method (CAM-B3LYP). *Chem. Phys. Lett.* **2004**, *393*, 51−57.
(53) Hehre, W. J.; Stewart, R. F.; Pople, J. A. Self-Consistent Molecular-Orbital Methods. I. Use of Gaussian Expansions of Slater-Type Atomic Orbitals. *J. Chem. Phys.* **1969**, *51*, 2657−2664.
(54) Lee, C.; Yang, W.; Parr, R. G. Development of the Colle-Salvetti Correlation-Energy Formula into a Functional of the Electron Density. *Phys. Rev. B: Condens. Matter Mater. Phys.* **1988**, *37*, 785−789.
(55) Furche, F.; Ahlrichs, R. Adiabatic Time-Dependent Density Functional Methods for Excited State Properties. *J. Chem. Phys.* **2002**, *117*, 7433−7447.
(56) Scalmani, G.; Frisch, M. J.; Mennucci, B.; Tomasi, J.; Cammi, R.; Barone, V. Geometries and Properties of Excited States in the Gas Phase and in Solution: Theory and Application of a Time-Dependent Density Functional Theory Polarizable Continuum Model. *J. Chem. Phys.* **2006**, *124*, 094107.
(57) Frisch, M. J.; Trucks, G. W.; Schlegel, H. B.; Scuseria, G. E.; Robb, M. A.; Cheeseman, J. R.; Scalmani, G.; Barone, V.; Mennucci, B.; Petersson, G. A.; et al. *Gaussian 09*; Gaussian, Inc.: Wallingford, CT, 2009.
(58) Kuhn, W. Über Das Absorptionsspektrum Der Polyene. *Helv. Chim. Acta* **1948**, *31*, 1780−1799.
(59) Kuhn, H. A Quantum-Mechanical Theory of Light Absorption of Organic Dyes and Similar Compounds. *J. Chem. Phys.* **1949**, *17*, 1198−1212.



DOI: 10.1021/acs.jpclett.8b00653
*J. Phys. Chem. Lett.* 2018, 9, 2460−2468